Mechanisms for the Origin of Mid-Ocean Ridge Axial Topography: Implications for the Thermal and Mechanical Structure of Accreting Plate Boundaries

JASON PHIPPS MORGAN

Department of Earth, Atmospheric, and Planetary Sciences, Massachusetts Institute of Technology, Cambridge

E.M. PARMENTIER AND J. LIN

Department of Geological Sciences, Brown University, Providence, Rhode Island

To better understand the implications of ridge axis morphology for the thermal and mechanical structure of accreting plate boundaries, we examine mechanisms for the creation of stress-supported axial topography and its dependence on parameters such as spreading rate, asthenosphere viscosity, and plate thickness near the ridge axis. Three basic mechanisms are considered: (1) asthenospheric upwelling in a narrow, steady-state conduit beneath a ridge axis; (2) mantle flow stresses due to plate spreading, extending ridge axis lithosphere, or melt segregation and associated mantle compaction; and (3) topography supported by moments due to horizontal extensional stresses in a thickening lithosphere. If mid-ocean ridge topography is due to asthenosphere rising in a narrow conduit at the ridge axis, then the conduit structure cannot be thermally controlled, as the associated thermal structure has relatively broad, flat isotherms instead of a conduitlike shape. Mantle flow associated with plate spreading alone induces no stress-supported topography. Thus the intuitive notion that diverging flow at the ridge axis due solely to plate spreading produces the axial valley is incorrect. Vertical mantle flow at the base of a stretching, accreting lithosphere and mantle flow associated with melt segregation can, however, lead to stress-supported axial topography. However, for these mantle flow related processes to produce significant amounts of axial relief, the mantle viscosity beneath the ridge axis must be on the order of 10^{20} Pa s (10^{21} P (poise)), significantly higher than generally accepted values of 10^{18} Pa s (10^{19} P). Horizontal extensional stresses in a strong, brittle lithosphere that thickens with distance from the ridge axis can produce axial topography of the form and amplitude observed on slow spreading ridges. A continuum idealization of deformation due to faulting is used to examine this mechanism. This model predicts the axial valley width is controlled by the plate thickness near the ridge axis. An 8-km-thick plate near the ridge axis would produce the 30-km-wide axial valley observed at slow spreading ridges. An increased lithosphere thickness of only several kilometers over the half-width of the axial valley can produce kilometer-scale relief. To examine whether a plate 8-10 km thick at the ridge axis that thickens by several kilometers within 15 km of the axis is plausible at a slow spreading ridge, thermal models that include both the heat of magmatic crustal accretion on the ridge axis and upwelling mantle flow beneath the axis are formulated. Hydrothermal cooling that increases the effective conductivity by about a factor of 10 is required for an 8-km-thick plate to exist at a slow spreading ridge axis. However, even with this enhanced hydrothermal cooling, the plate thickness at a fast spreading ridge axis and the resulting horizontal force in the plate are too small to result in appreciable topography. While mid-ocean ridge axial topography is strongly influenced by spreading rate, other factors also shape axial structure. For example, the anomalously shallow slow spreading Reykjanes Ridge has an axial structure more like that of a fast spreading ridge, and the anomalously deep intermediate spreading Australian-Antarctic Discordance has a median valley axial structure typical of a slower spreading ridge. In addition, within a given spreading segment there is often a systematic deepening of the ridge axis toward transform offsets. These non-spreading-rate-dependent axial topographic variations may be produced by variations in magmatic heat input associated with crustal emplacement which shapes the thermal structure and lithosphere thickness near the ridge axis.

INTRODUCTION

The well known difference in the axial topography of slow and fast spreading mid-ocean ridges is shown in Figure 1 by typical topographic profiles across the axes of slow, medium, and fast spreading ridges. The characteristic 1-km-deep axial valley and flanking crestal mountains that form at slow spreading rates do not exist at faster spreading rates, where instead relatively low relief axial topography is observed. Although this spreading rate dependence of ridge axis morphology is widely recognized, there still are no conclusive explanations of why an axial valley exists at

slow spreading rates but vanishes at faster spreading rates. Since seafloor bathymetry is the most frequently acquired and widely available geophysical data, it is also important to understand the possible implications of ridge axis topography for the thermal and mechanical structure of accreting plate boundaries.

In the few areas where data of sufficient quality and resolution have been obtained, gravity anomalies provide an important observational constraint on the origin of the axial valley and particularly the possible role of crustal thickness variations in producing the axial valley topography. Gravity data for a segment along the Mid-Atlantic Ridge from about 13° to 15°N has been reported by Collette et al. [1980]. The amplitude of the observed gravity anomaly shows that the ridge axis topography cannot be isostatically compensated at a depth as shallow as 6-8 km and so cannot
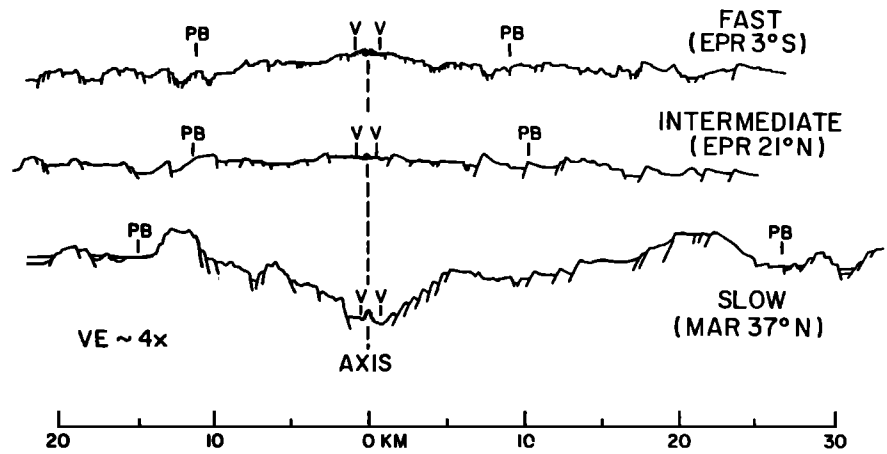
Macdonald (1982)

Fig. 1. Axial topography along profiles perpendicular to typical slow (5-25 mm/yr), intermediate (25-45 mm/yr), and fast (>45 mm/yr) spreading ridge axes from Macdonald [1982]. A 1- to 2-km-deep, 30-km-wide axial valley with flanking crestal highs is present at slow spreading ridges. At faster spreading rates the axial topography is much more subdued. The symbols V and PB on the profiles delineate the width of the region of active volcanism along the spreading center and the boundaries of the region of active faulting, respectively. EPR is East Pacific Rise; and MAR, Mid-Atlantic Ridge. The profiles have a vertical exaggeration (VE) of 4.

be explained by crustal thickness variations [Collette et al., 1980; Parmentier and Forsyth, 1985]. Furthermore, seismic refraction studies along the Mid-Atlantic Ridge [Purdy and Detrick, 1986; Louden et al., 1987] do not show abnormally thin crust beneath the axial valley. Thus, both gravity and seismic refraction studies indicate that the crust within the axial valley is essentially the same thickness as that of older seafloor. Therefore, the axial valley must be a dynamically maintained, stress-supported topographic feature.

In this paper we examine simple models for the origin of ridge axis topography. While a number of previous models have been presented, these models do not generally provide a clear indication of the origin of vertical forces responsible for the large-amplitude topography at slow spreading ridge axes. To provide a framework and motivation for our discussion of simple models, we begin by reviewing previous models for slow spreading ridge structure.

PREVIOUS MODELS FOR AN AXIAL VALLEY

Sleep [1969] and Lachenbruch [1973, 1976] have suggested that the structure of a slow spreading ridge axis consists of a vertical conduit through which asthenosphere rises to form a thick plate near the ridge axis. This is presently the only model which explicitly addresses the origin of vertical forces producing the axial valley morphology. In this model, the viscous pressure drop associated with vertical flow in the conduit creates the axial valley depression. Vertical forces resulting from shear stresses on the conduit walls support the elevated flanking crestal mountains. The principal difficulty of the steady-state conduit model is to explain the existence of a conduit in terms of thermal structure and reasonable rheological behavior. Specifically, if the lithosphere forms by conductive cooling and the strength or viscosity of mantle rock is primarily a function of temperature, then a conduit of the type envisioned by these studies should not form. This is shown by the example in Figure 2. The methods used to obtain this result will be discussed later. In this example, the plate thickness is

prescribed so that the horizontally moving plate thickens rapidly with distance from the ridge axis, forming a conduit at the axis with a width that is comparable to the width of an axial valley. Flow in a mantle half-space of uniform viscosity occurs due to both the horizontal motion and accretion of the plate. The steady-state thermal structure based on these velocities is shown by isotherms at specified fractions of the deep mantle temperature T_m. The shape of the bottom of the plate clearly differs greatly from that of the isotherms. While the localized upwelling at a ridge axis due to the presence of a conduit transports heat into the region beneath the ridge axis, cooling within the rigid plate is due primarily to vertical heat conduction, resulting in the shallow, gently sloping isotherms shown in Figure 2. The release of latent heat beneath the ridge axis would raise the temperature and elevate isotherms to shallower depths. The isotherms would, however, maintain their gently sloping character since this is controlled by vertical heat conduction. The above results indicate that no conduit would be present if the viscosity of mantle rock depends primarily on temperature.

It has frequently been suggested that a conduit could form due to a weakening effect of partial melt or water. However, studies of magma migration suggest that even small amounts of melt forming a connected network can rapidly migrate out of a solid matrix. Studies of the strength of olivine containing basalt melt [cf. Cooper and Kohlstedt, 1986] suggest that the principal effect of small amounts of melt will be to enhance deformation related to grain boundary diffusion. For deformation that occurs by a combination of dislocation creep and grain-boundary diffusion, the presence of a few percent melt enhances the deformation rate only by a factor of 2-5 [Cooper and Kohlstedt, 1986]. A recent study [Karato, 1986] suggests that the presence of a small amount of melt may actually strengthen partially molten rock because water, which weakens mineral grains, is partitioned into the melt. Therefore while the effect of partial melting on the strength of rock is not fully resolved, our
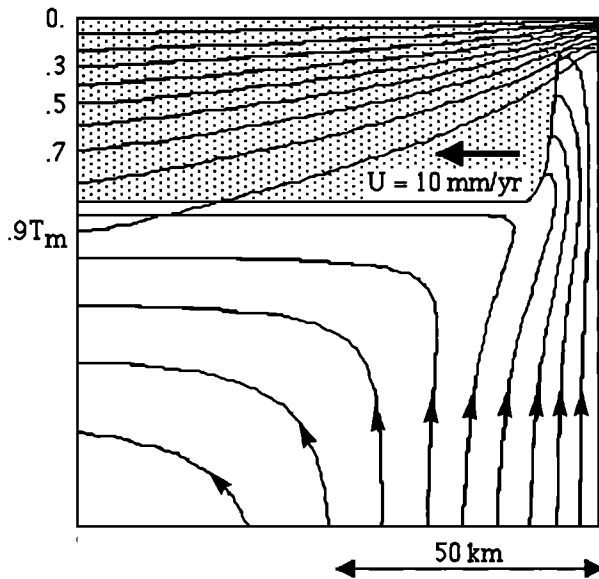
Fig. 2. Thermal and mechanical structure of a slow spreading mid-ocean ridge with a prescribed conduitlike mechanical structure. The lithosphere (dot shaded) moves horizontally and thickens rapidly near the ridge axis forming a conduit. Streamlines show viscous flow beneath the plate due to plate motion and accretion assuming the mantle is a uniform viscosity half-space. The thermal structure corresponding to this velocity field is shown by isotherms at specified fractions of the deep mantle temperature T_m. The bottom of the lithosphere clearly does not correspond to an isotherm, thus a steady-state ridge axis conduit cannot be present if the strength or viscosity is solely a function of temperature.

current understanding indicates that small amounts of partial melt will not reduce the strength by the several orders of magnitude that would be needed to form a ridge axis conduit.

Compositional change resulting from melt extraction will raise the solidus temperature and therefore the viscosity of the residual mantle rock. The viscosity due to thermally activated creep is proportional to $\exp(AT_m/T)$ where $A \sim 40$ and T_m is the melting temperature [e.g., *Brace and Kohlstedt*, 1980]. Thus, if melting increases T_m by 100°C as suggested from petrologic studies, this would increase the viscosity by approximately two orders of magnitude. While this effect has not been previously considered, it is potentially important and could result in the formation of the strong lithosphere forming conduit walls [cf. *Lachenbruch*, 1973]. Alternatively, if the composition changes affect the solid fraction of conduit mantle and the presence of melt does not significantly reduce the viscosity, this effect could actually increase the viscosity of material in the conduit.

It is also important to question whether a conduitlike thermal structure may result from hydrothermal cooling. This question will be explored in more detail later, but hydrothermal cooling that is simply described by an enhanced thermal diffusivity will produce even flatter isotherms in the mantle beneath the ridge axis. The simple example in Figure 2 does not prove that a steady-state conduit cannot exist, but shows that special assumptions about mantle rheology or hydrothermal cooling are required.

Tapponier and Francheteau [1978] first suggested steady-state necking as a conceptual model for slow spreading ridge axes. Their model consists of two parts: first, that extension of the plate creates a seafloor depression at the ridge axis and, second, that this depression is regionally compen-

sated by elastic flexure of the lithosphere producing the flanking uplift of the crestal mountains. This is essentially the Vening Meinesz [1950] model for rifts. In its application to mid-ocean ridges, the model does not explain the amplitude and width of the ridge axis depression in terms of other physical variables, such as extension rate and plate thickness. Furthermore, a variety of evidence suggests that the lithosphere deforms by faulting near the ridge axis. Studies of seafloor structure [*Macdonald and Luyendyk*, 1977; *Macdonald and Atwater*, 1978; *Laughton and Searle*, 1979; *Macdonald*, 1982] have concluded that axial valley relief is a consequence of faulting. Studies along the Mid-Atlantic Ridge south of the Kane fracture zone [*Toomey et al.*, 1985] show that seismicity extends to depths of about 8 km and that microearthquakes occur beneath both the axial valley floor and the crestal mountains. Deformation due to faulting is not well described by simple elastic flexure.

The numerical models of *Sleep and Rosendahl* [1979] were the first to include the effects of a viscoplastic plate and quantitatively predict the formation of an axial valley. However, the geologiclike complexity of the assumed thermal and rheological structure combined with limited numerical resolution does not permit a simple understanding of the mechanism(s) causing the calculated axial valley morphology.

Our approach has been to examine simple models which isolate potentially important physical mechanisms causing seafloor topography near a ridge axis. We will show that horizontal extensional stresses in a strong continuously deforming plate near the ridge axis can produce an axial valley-like ridge axis morphology. Stresses due to mantle flow and melt segregation beneath an extending plate can produce a similar morphology, but a mantle viscosity significantly higher than generally accepted values would be required to explain the observed axial valley relief.

TOPOGRAPHY DUE TO MANTLE FLOW STRESSES

If lithospheric stretching is occurring near the ridge axis, then either vertical mantle flow or magma intrusion into the stretching lithosphere is required to balance lithospheric thinning due to stretching and thus maintain a steady-state lithosphere thickness distribution. Vertical mantle flow at the base of a stretching and accreting lithosphere is capable of producing stresses that can support ridge axis topography [*Phipps Morgan and Parmentier*, 1984]. However, in the following analysis we will show that mantle flow can create a significant axial valley depression only if mantle viscosities beneath the ridge axis are at least two orders of magnitude larger (10^{20} Pa s or 10^{21} P) than commonly accepted values (10^{18} Pa s or 10^{19} P). Mantle flow will be induced by both vertical and horizontal motion at the bottom of the lithosphere and by melt segregation. We will first consider mantle flow induced by motion at the bottom of the lithosphere and discuss the effects of melt segregation on mantle flow in the following section.

Consider flow in a mantle half-space of uniform viscosity beneath a planar, horizontal lithosphere-asthenosphere boundary. Flow in the half-space induced by vertical and horizontal flow along the top, $z=0$, can be represented as a superposition of Fourier harmonics in the horizontal x coordinate. For each Fourier component of horizontal or vertical velocity on the top of the mantle half-space, u or w
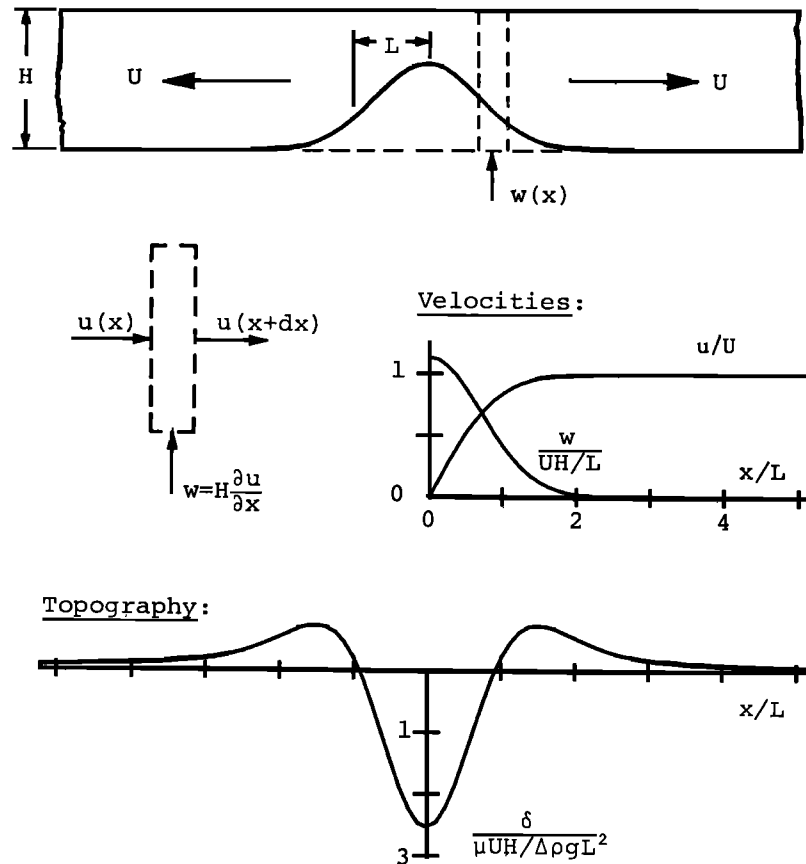
Fig. 3. Axial topography due to vertical mantle flow at the base of extending lithosphere. (Top) Model in which extending lithosphere thickens slowly with distance from the ridge axis. The thickness variation shown is exaggerated for clarity. (Middle) Vertical mantle flow w across the approximately planar base of the lithosphere (dashed line) can be found by considering flow into the base of a stretching column of lithosphere with horizontal velocity $u(x)$ that is needed for steady-state material conservation. The assumed error function plate spreading distribution, corresponding to a Gaussian upwelling distribution, produces the axial topography shown. (Bottom). Here δ is the topography, μ is the mantle viscosity, U is the half-spreading rate, H is the plate thickness in the stretching region, L is the half-width of the stretching region, $\Delta\rho = \rho_m - \rho_w$ is the difference between mantle and water densities, and g is the acceleration of gravity.

respectively, the induced normal and shear stresses on the top of the half-space are $\sigma_{xz} = -2\mu ku$ and $\sigma_{zz} = -2\mu kw$, where k is the wavenumber. The stresses resulting from any prescribed distribution of horizontal or vertical velocity can be obtained by the superposition of Fourier components. Thus any horizontal distribution of velocity ($w=0$) on the top of the mantle half-space will produce flow-induced shear stresses at the bottom of the lithosphere but no vertical normal stresses that can support seafloor topography. This simple result contradicts the intuition that the diverging flow due to plate spreading will produce an axial valley hole at the ridge axis [cf. *Nelson*, 1981].

For a lithosphere-asthenosphere boundary that is nearly but not exactly planar, mantle flow into a stretching steady-state lithosphere can be approximated as shown in Figure 3. The net upward flow is simply the difference in the horizontal flow entering and leaving a thin vertical slice of height H, so $w|_{z=0} = H\partial u/\partial x$, where H is the lithosphere thickness outside the axial region of stretching and accretion. With a prescribed spreading velocity $u=U\mathrm{erf}(x/L)$, the calculated normal-stress-supported topography is shown in Figure 3. Stresses resulting from the prescribed vertical velocity were calculated using a standard fast Fourier transform (FFT) algorithm with 256 uniformly distributed points. For a mantle

viscosity $\mu=10^{21}$ P (10^{20} Pa s), an axial valley half-width $L=15$ km, a ridge axis lithosphere thickness $H=8$ km, and a half spreading rate $U=20$ mm/yr (20 km/m.y.), this mechanism predicts a 1-km-deep stress-supported axial valley. Smaller mantle viscosity, smaller lithospheric thickness near the ridge axis, and smaller amounts of lithospheric stretching would all reduce the amplitude of the topography. Note that in calculating the seafloor topography, mantle flow induced normal stresses are assumed to be supported only by buoyancy forces arising from topography at the crust-water boundary with no contribution from the strength of the lithosphere. This will overestimate the topography if some of the vertical force at the bottom of the plate is supported by stresses within the plate.

To consider lithosphere thickness variations in the more general case of a highly nonplanar lithosphere-asthenosphere boundary and to assess the accuracy of the above approximation of a nearly planar boundary, boundary element solutions for the mantle flow induced normal stress distribution were obtained for the several plate thickness distributions shown in Figures 4a-4d. For this problem, the boundary element method (BEM) has two basic advantages over other methods: (1) for arbitrarily shaped two-dimensional regions it is a simpler task to discretize a one-dimensional
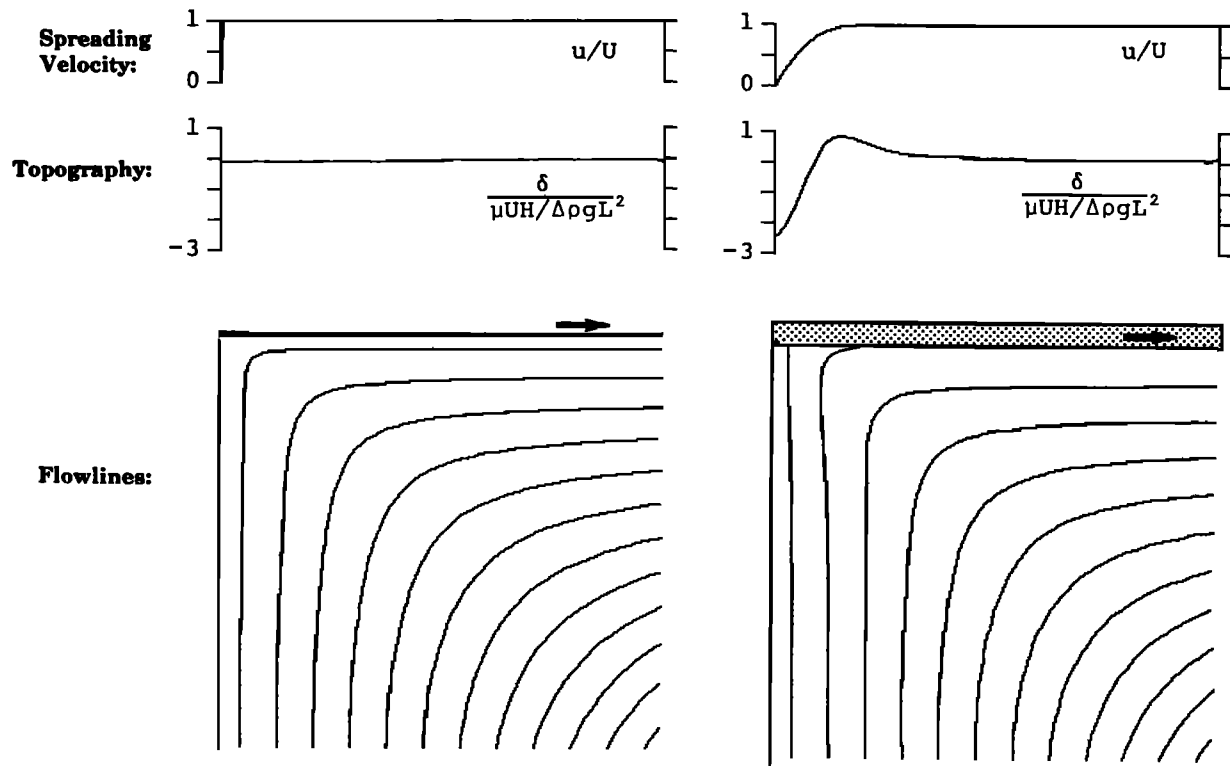
Spreading Velocity:

u/U

Topography:

$\dfrac{\delta}{\mu UH/\Delta\rho g L^2}$

Flowlines:

Fig. 4a

Fig. 4b

Spreading Velocity:

u/U

Topography:

$\dfrac{\delta}{\mu UH/\Delta\rho g L^2}$
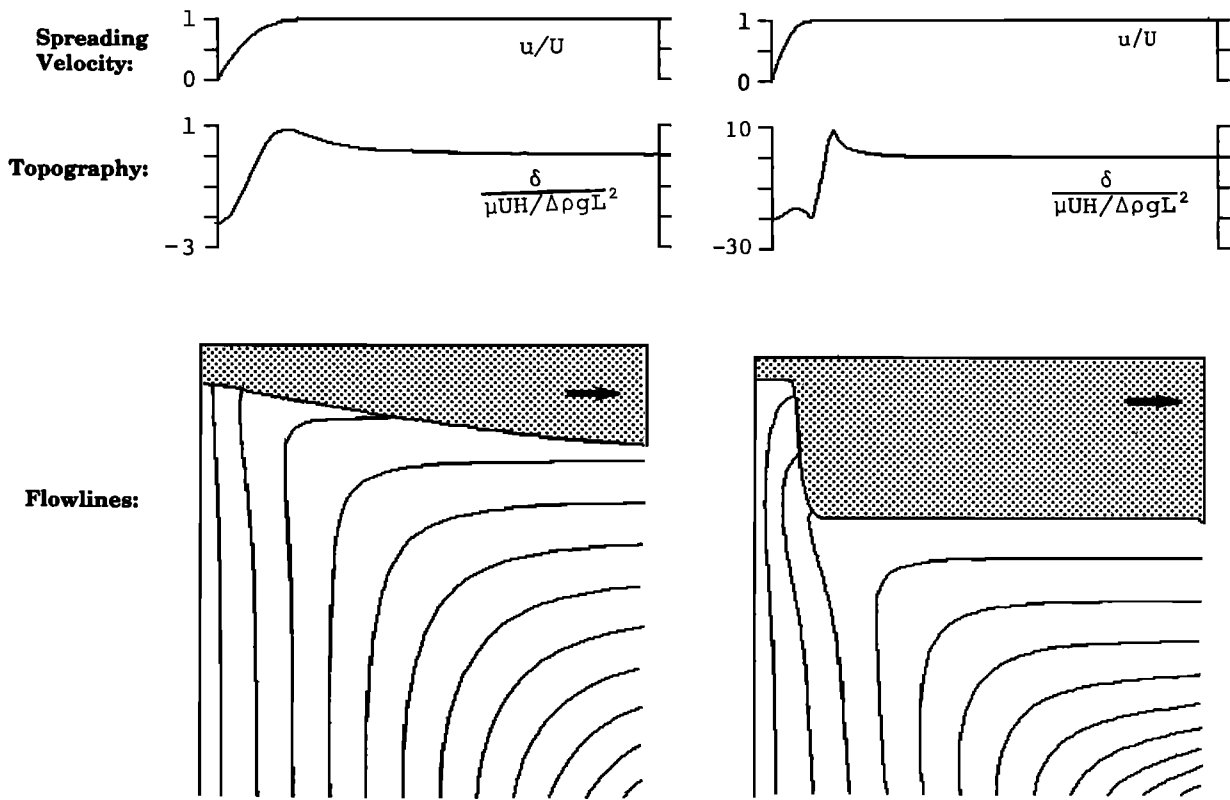
Flowlines:

Fig. 4c

Fig. 4d

Fig. 4. Mantle flow and axial topography for several prescribed distributions of lithosphere (dot shaded) thickness and horizontal extension rate. Spreading velocity distribution and corresponding topography are shown at the top of each figure. Streamlines of the mantle flow are shown at the bottom of each figure. Symbols and notation are the same as in Figure 3. (a) Constant thickness lithosphere that is emplaced entirely at the ridge axis and spreads with a uniform velocity. (b) Constant thickness, stretching and accreting lithosphere equivalent to the model of Figure 3. (c) Slowly thickening stretching and accreting lithosphere. (d) Ridge axis conduit with corresponding thermal structure shown in Figure 2.

boundary than the whole two-dimensional region, and (2) there are no numerical complications needed to enforce the incompressibility condition. The BEM is an extremely convenient technique for solving problems in a piecewise homogeneous medium where an exact Green's function solution is known. In the BEM, this singular solution is integrated to find the solution for a particular Green's function distribution over a line segment; for example a constant, linear, or quadratic distribution could be employed. The boundary is discretized into a finite number of boundary line segments or elements, and influence coefficients are calculated that relate the contribution to the stresses and velocities on one element from given stresses or velocities acting along another element. In the present application of the BEM, each boundary element is a line segment with a uniform distribution of normal and tangential force acting along it. This results in unknown normal and tangential force magnitudes for each element. The velocity or stress distribution along the boundary is prescribed, and with velocities evaluated at the center of each element, the distribution of boundary forces which will produce this prescribed boundary velocity and stress distribution at each element midpoint is calculated by solving a linear system of equations for the unknown magnitudes of the boundary force distribution for each boundary element. The known boundary force distribution can then be used to calculate the stresses or velocities at any point within the region.

The program (TWOFS) used in the present study is described by Crouch and Starfield [1983], who also present a more complete development of the BEM. The following boundary conditions are prescribed. (1) Along the lithosphere-asthenosphere boundary, velocities are set to the horizontal plate velocity $u(x)$ and vertical velocity due to stretching $w(x) = H(x)\partial u/\partial x$. (2) Along the ridge axis ($x=0$) a symmetry condition is assumed ($u=0$, $\tau_{xz}=0$). Computationally, elements on the right-hand side of the ridge axis which mirror those on the left-hand side of the ridge axis are constructed. Because of this symmetry only unknowns for the right-hand side of the ridge axis need be computed, and no boundary elements are needed on the vertical boundary directly beneath the axis. (3) Along the bottom of the box, stress-free boundaries are assumed. (4) At the right-hand side of the box ($x=L$) the horizontal and vertical velocities are prescribed as the solution for a planar half-space with a uniform horizontal velocity along the top which is at a depth $H(L)$. At least 50 elements along the top and 40 elements along the right side and bottom were used. Boundary element solutions will be least accurate near the boundaries of the region, where the assumed discontinuous force distribution is an imperfect approximation to continuous velocity or stress boundary conditions. However, according to Saint Venant's principle, solutions will become increasingly accurate away from the boundaries of the region. From the agreement between boundary element and semi-analytical FFT solutions for the planar half-space problem (Figures 3 and 4b), stresses at the element midpoints along the lithosphere-asthenosphere boundary are expected to be accurate to better than 5% for all the lithosphere thickness distributions shown in Figure 4.

Figure 4c shows the mantle flow and associated axial topography due to stretching and accretion of a variable thickness lithosphere. This is almost identical with the earlier result of Figure 3 which assumes a nearly planar litho-

sphere-asthenosphere boundary. To compare the two results, an average lithosphere thickness in the stretching region $H^* = \int w(x)H(x)dx/\int w(x)dx$ can be defined. The calculated ridge axis topography for a slowly varying thickness $H=H(x)$ and $w=H\partial u/\partial x$ in Figure 4c is almost identical in both form and amplitude to that calculated with a constant lithosphere thickness $H=H^*$ and $w=H^*\partial u/\partial x$ (Figure 3 or 4b).

The component of mantle deformation that produces axial valley-like topography can be seen in the mantle streamlines of Figure 4. The streamlines beneath the ridge axis converge as they near the base of the lithosphere, indicating a vertical stretching of the mantle beneath the ridge axis. The corresponding tensional vertical deviatoric normal stress supports the axial valley depression.

For large variations in lithosphere thickness near the ridge axis, as in the case of a ridge axis conduit, the approximations of a nearly planar lithosphere-asthenosphere boundary break down. Boundary element solutions can still be obtained for these cases. The example in Figure 4d shows that the presence of a conduit localizing upward mantle flow at the ridge axis greatly increases the predicted ridge axis topography. The increase over that in Figure 4c is by about a factor of 10 for this particular lithosphere thickness distribution.

TOPOGRAPHY DUE TO MELT SEGREGATION

The steady state segregation of melt from mantle matrix and the resulting matrix compaction due to the loss of melt volume will create an effective volume sink within the mantle. The mantle flow to fill in this mass deficit in the segregating and compacting region can produce axial topography. Melt segregation and associated mantle compaction is idealized as occurring at a single line sink beneath the ridge axis. The line sink may be regarded as a small compacting region of cylindrical cross section. A more realistic segregating and compacting region can be constructed by superimposing these line sink solutions. The normal-stress-supported topography due to a line sink at a depth D beneath the surface of a viscous halfspace, in this case the crust-mantle boundary at the ridge axis, can be found by adding a line sink solution at a depth D below the surface to an image sink a distance D above the surface. The resulting normal-stress-supported topography is shown in Figure 5. For a melt removal rate equal to the crustal production rate $2UH$ at the ridge axis, where H is the crustal thickness and U is the half-spreading rate, the maximum axial valley depression is approximately $\mu UH/\Delta \rho g D^2$, where $\Delta \rho = \rho_m - \rho_w$, μ is the viscosity of the mantle matrix, g is the acceleration of gravity, and D is the depth to the segregating region.

This solution, which is formed by superimposing two line sinks [cf. Batchelor, 1967, p. 89], produces the correct normal stress but satisfies a shear stress-free boundary condition instead of a no horizontal velocity boundary condition at the surface of the half-space. To solve for the contribution to mantle flow from melt segregation beneath a spreading center, a complementary solution to cancel the horizontal flow generated at the crust-mantle boundary by the two line sink solution must be added to this solution. This complementary solution can be obtained by the complex-variable techniques developed, for example, by Muskhelishvili [1953, p. 584]. Since it involves only horizontal flow at the surface of the half-space, this comple-
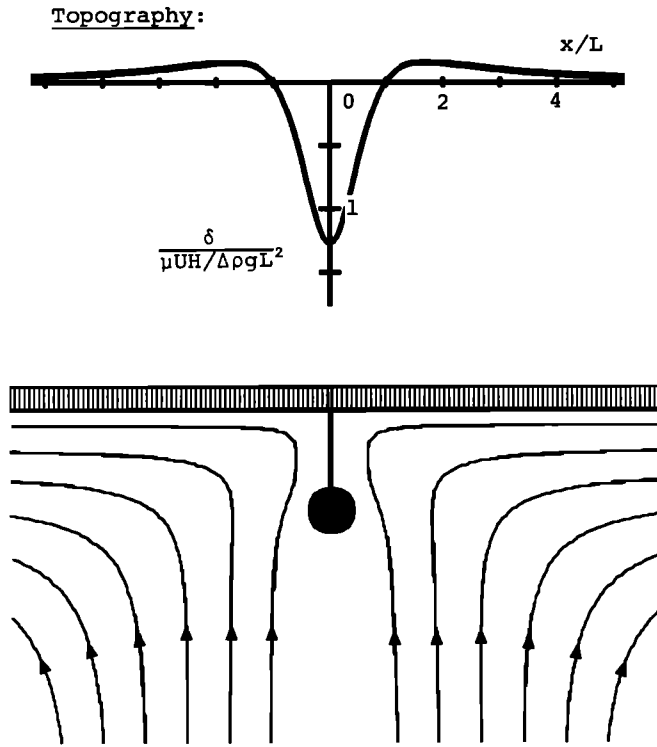
Topography:

Fig. 5. (Top) Axial topography due to mantle flow into a small cylindrical region (line sink) of melt segregation. Here δ is the topography, μ is the mantle viscosity, U is the half-spreading rate, H is the crustal thickness, L is the depth to the segregating region, and $\Delta\rho = \rho_m - \rho_w$. More complicated and realistic distributions of melt segregation could be constructed by superimposing line sink solutions. (Bottom) Streamlines of mantle flow due to plate spreading and melt segregation with associated mantle matrix compaction. Analytical solution for mantle flow due to line sink melt segregation is given in text. Note, by comparing with Figure 4a, that melt segregation localizes upwelling beneath the ridge axis.

mentary solution does not contribute to the surface normal stress. The mantle flow due to melt segregation in a line sink beneath a spreading center is found by adding the two line sink and complementary solutions

$$u+iw = \frac{m}{\pi}\{\frac{1}{2}[\frac{iz_1 - \zeta}{z^2 + \zeta^2} + \frac{iz_1 - \bar{\zeta}^2}{z^2 + \bar{\zeta}^2}] + iz[\frac{iz_1 - \zeta}{z^2 + \zeta^2}]^2\}$$

$$+ \frac{m}{\pi}\{\frac{1}{2}[\frac{x}{x^2 + (z-z_1)^2} + \frac{x}{x^2 + (z+z_1)^2}]$$

$$+ \frac{i}{2}[\frac{z-z_1}{x^2 + (z-z_1)^2} + \frac{z+z_1}{x^2 + (z+z_1)^2}]\}$$

where u and w are velocities in the x (horizontal) and z (vertical) directions, respectively, and m is the melt segregation rate into a line sink a depth z_1 beneath the surface of the half-space or crust-mantle boundary. The complex variables $\zeta = x+iz$ and $\bar{\zeta} = x-iz$, where x is the real and z is the imaginary part of the complex variable, have been used to concisely express the solution.

The normal stress-supported axial topography produced by melt compaction may be substantial if melt removal occurs at shallow depth beneath the ridge axis and if ridge axis asthenosphere viscosities are on the order of 10^{20} Pa s (10^{21} P). Since, as shown in Figure 5, the depth to the segregating region is the half width of the resulting topographic feature, melt removal occurring in a cylindrical region cen-

tered 15 km beneath the crust-mantle boundary would produce a 30-km-wide axial valley. For a mantle viscosity of 10^{20} Pa s, a 1-km-deep axial valley will result from an along-axis crustal production rate $m = 2UH = 230$ m²/yr corresponding to $U = 20$ mm/yr and $H = 6$ km. Melt segregation occurring at greater depths will produce a broader and shallower axial valley for otherwise identical model parameters. For a similar mantle viscosity, depth of melt segregation, and crustal thickness, ridge axis topography associated with melt segregation should be greater on faster spreading ridges. If crustal thickness and mantle viscosity are approximately the same on fast and slow spreading ridges, a larger-amplitude topography at slower spreading rates could be explained by shallower or more localized melt segregation. However, melt segregation can contribute significantly to axial topography only if there is a strong localization of melt segregation and the asthenosphere is more viscous (10^{20} Pa s) than it is usually thought to be (10^{18} Pa s). Streamlines in Figure 5 show the flow in a mantle half-space due to melt segregation in a small cylindrical region 30 km beneath the crust-mantle boundary combined with flow due to plate spreading. The plate spreading flow is described by vertical and horizontal velocities $u = 2U[\tan^{-1}(x/z)-xz/(x^2+z^2)]/\pi$ and $w = -2Uz^2/[\pi(x^2+z^2)]$, respectively, with streamlines shown in Figure 4a. Note that flow induced by melt segregation and associated mantle compaction tends to localize the region of mantle upwelling beneath the ridge axis as shown by comparing the streamlines in Figure 5 with those in Figure 4a.

RIDGE AXIS TOPOGRAPHY DUE TO PLATE EXTENSIONAL STRESSES

Ridge axis topography can also be produced by horizontal extensional stresses in a strong plate that thickens with distance from a ridge axis [Parmentier et al., 1985; Lin and Parmentier, 1986; Parmentier, 1987]. A perfectly plastic material is considered as a continuum description of deformation due to slip on many closely spaced faults. The strength of the plate in this case arises from the frictional resistance to slip on the faults. Simple models to examine the form and amplitude of ridge axis topography will consider a prescribed plate thickness variation. With the bottom of the strong plate defined by a prescribed temperature, the plate thickness variation will be controlled by thickening of the plate due to cooling away from the ridge axis and by localized thinning of the plate near the ridge axis due to plate extension. As discussed later, plate extension of the magnitude inferred from seafloor faulting and seismic moment release will make a smaller contribution than cooling to plate thickening away from the axis. Thermal models to examine plate thickness variation are described in a later section.

The mechanism producing topography as a variable thickness plate extends can be understood qualitatively from Figure 6a. Because the plate thickness varies, the horizontal force F within the plate acts at different depths on the two vertical sides of a material column, thus creating a moment M. This moment, distributed horizontally over the region where the thickness varies, bends the plate. The vertical force due to the resulting seafloor topography must balance the applied moment and thus has the form shown: a central depression with flanking uplifts. Since there is no net vertical force acting on the plate, only moments, the topogra-
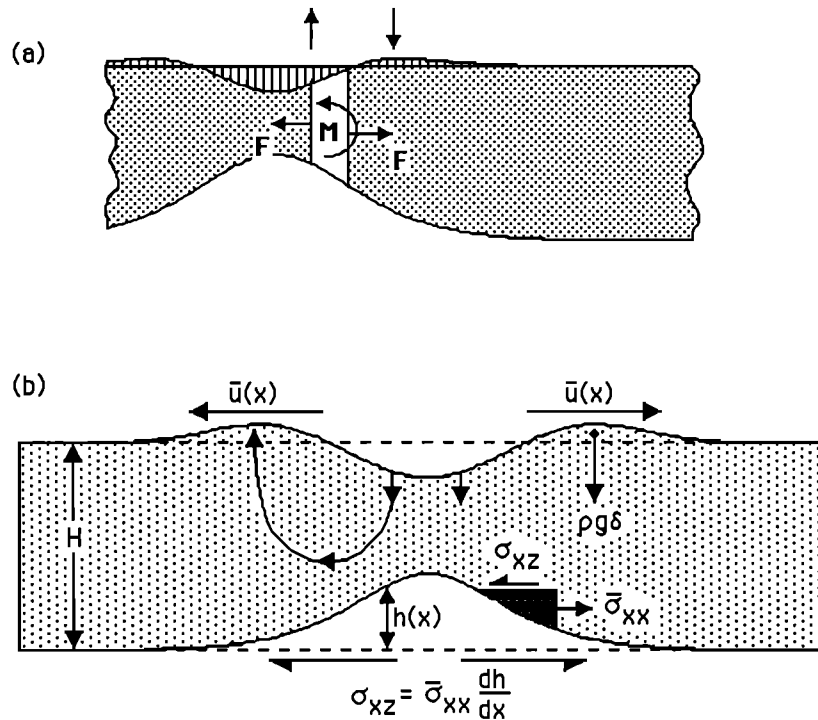
Fig. 6. (a) Force (F) and moment (M) distribution can produce axial topography by flexural deformation of a strong viscous or plastic plate of variable thickness that is being pulled apart by external forces. Plate thickness variations result in changes in depth of the horizontal force, thus creating moments within the plate that must be balanced by moments due to topographic forces resulting from flexural deformation. (b) For a strong plate with slowly varying thickness, stresses due to changes in plate thickness can be represented by an effective shear stress σ_{xz} acting on the base of the plate. Consider the horizontal force balance on the darkly shaded triangular material element: the horizontal force $\sigma_{xx}\,dh$ acting on the vertical side of this triangle must be balanced by the force $\sigma_{xz}\,dx$ acting along the horizontal side. Because the mantle is assumed to be a very weak fluid, no horizontal forces act on the hypotenuse of the triangle. This force balance shows that the induced shear stress σ_{xz} is given by the product of the mean tensile stress σ_{xx} and the rate of change in plate thickness $\partial h/\partial x$. The shear stress σ_{xz} produces internal deformation shown by the schematic streamline. See text for further discussion.

phy averaged across the ridge axis must vanish. Deformation of the plate in response to the applied moments could be approximated as flexure of a viscous or plastic plate. However, since the half width of an axial valley is not large compared to the plate thickness, a more accurate description of the topography can be obtained by considering two dimensional deformation or flow within the plate rather than flexural approximations.

As shown in Figure 6b, consider a strong plate of perfectly plastic material that rests on a very weak fluid mantle substrate. The presence of a horizontal applied stress σ_{xx} that causes extension of the plate results in an induced shear stress σ_{xz} that is required to maintain equilibrium of the small, darkly shaded material element at the bottom of the layer. This induced shear stress causes flow within the layer which is superimposed on the flow due to horizontal extension and which results in a central depression and flanking uplifts. When the plastic plate is kept at yield by the applied stress σ_{xx}, stresses due to gravitational attraction on the topography at the top surface of the layer also cause flow which opposes that of the induced shear stress. For a prescribed plate thickness variation $h(x)$, the equilibrium topography will be that for which the vertical velocity at the upper surface vanishes.

Flow within the plate is described by the equilibrium equations and the incompressibility condition. To obtain analytical solutions, the thickness variation $h(x)$ is assumed

to be small compared to the plate thickness so that the induced shear stress can be applied at the bottom of a layer of uniform thickness H. This approximation has been frequently applied in theoretical studies of folding and boudinage. The strength of the plate and therefore σ_{xx} is also assumed to be independent of depth within the plate. The boundary conditions at the bottom of the layer ($z=H$) are $\sigma_{xz}=\sigma_{xx}\,\partial h/\partial x$ and $\sigma_{zz}=0$, and the boundary conditions at the top of the layer ($z=0$) are $\sigma_{xz}=\sigma_{xx}\partial\delta/\partial x$, $\sigma_{zz}=\Delta\rho g\delta$, and $w=\partial(u\delta)/\partial x$. The last equation states that the surface $z=\delta(x)$ is a particle path with material at the top of the plate moving along this surface. The perturbation flow due to the shear stress σ_{xz} at the bottom of the layer can be represented as a superposition of Fourier harmonics in the x direction. The velocity distribution associated with any horizontal wavenumber is given by solution of equations (10) and (11) of *Zuber and Parmentier* [1986].

Figure 7 shows the topography resulting from a prescribed plate thickness variation of the form $h\ \exp[-(x/L)^2]$ where the width of the plate thickness variation $L = 0.5H, H$, and $2H$. The surface topography and velocity distribution within the layer which satisfies the above boundary conditions were calculated using a standard FFT algorithm with 256 points uniformly distributed over the length of the examples shown. The amplitude of the relief is proportional to the magnitude of the layer thickness variation, h, and depends on a single dimensionless parameter $S=\sigma_{xx}/\Delta\rho gH$, where is
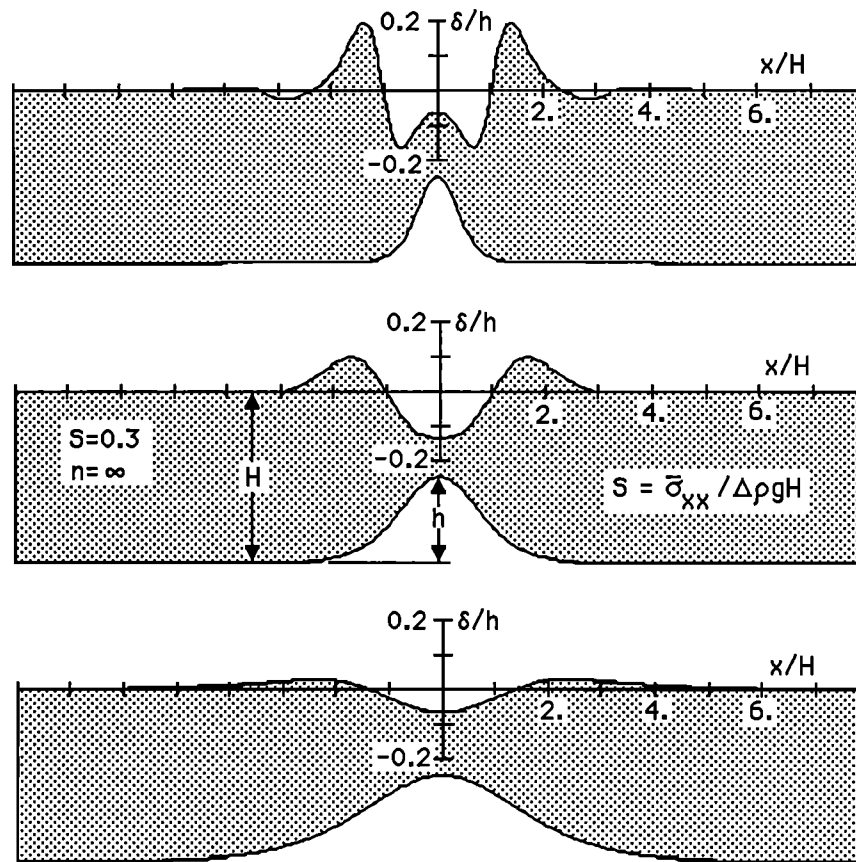
Fig. 7. Axial topography due to deformation resulting from horizontal extensional stresses in a lithosphere that thickens with distance from a ridge axis. The prescribed thickness variation is shown at the bottom of each figure and the resulting topography along the top. All cases consider a perfectly plastic lithosphere with the same value of the strength parameter S defined in the text. Different lithosphere thickness variations are considered by varying the half-width of the thickening region $L = 0.5H, H$, and $2H$.

the mean horizontal applied stress, $\Delta\rho = \rho_m - \rho_w$, g is the acceleration of gravity, and H is the lithosphere thickness near the ridge axis. Similar results for a range of S values shows that the amplitude of the relief is approximately proportional to S and inversely proportional to L. If the width of the plate thickness variation is comparable to or smaller than the plate thickness, the predicted width of the axial valley, measured from flanking high to flanking high, is 3-4 times the plate thickness. A wider plate thickness variation produces a broader axial valley, but the predicted width of the axial valley is not less than about four plate thicknesses. With a brittle plate thickness of about 8 km, as inferred from the depth of microseismicity on the axis of the Mid-Atlantic Ridge south of the Kane fracture zone [Toomey et al., 1985], the predicted flank to flank width of the axial valley would be about 30 km, which agrees well with the observed axial valley width along this segment of the ridge.

Frictional sliding on faults will result in a yield stress that increases linearly with depth [cf. Brace and Kohlstedt, 1980]. For faults containing hydrostatic water pressure and on which frictional sliding occurs with a laboratory-measured friction coefficient of 0.85 [Byerlee, 1978], the depth-averaged value of σ_{xx} is $S=0.4$. The absence of water pressure results in the larger value $S=0.7$. For $S=0.4$ results like those in Figure 7 predict seafloor topography with a relief of about 30% of the plate thickness variation. Therefore a plate thickness variation less than about 3 km is sufficient

to produce the 1 km of seafloor relief typically observed on slow spreading ridge axes.

RIDGE AXIS THERMAL MODELS

As an extending plate thickens with distance from the ridge axis, the dynamic consequences of the thickening of the deforming plate may create or at least contribute significantly to the axial morphology of slow spreading ridges. It is important to emphasize that the total amount of extension that accumulates in a thin vertical section of plate as it moves through the axial valley is relatively small. Based on observed distributions and heights of fault scarps, Macdonald and Luyendyk [1977] and Macdonald and Atwater [1978] estimate only 10-20% extension. Similarly, the average seismic moment release along slow spreading ridges, as reported by Solomon et al. [1986], can be interpreted to indicate that only 5-10% of the total spreading velocity is due to seismic fault slip. As seen at the seafloor, most of the plate spreading velocity develops within a 1- to 2-km-wide neovolcanic zone at the ridge axis where spreading is accommodated by dike intrusion. The spreading velocity increases only slightly away from the axis due to horizontal extension of the lithosphere. While the amplitude of the topography depends on the magnitude of plate thickness variation near the ridge axis, the plate thickness variation cannot be solely a result of plate extension. Extension will

tend to thin the plate, but if the above estimates of extension are correct, this effect must be relatively small. If the bottom of the strong, brittle plate is defined by a prescribed temperature, the thermal structure due to mantle flow beneath the ridge axis and crustal accretion on the axis will control the plate thickness variation.

A number of ridge thermal models have been presented in which the thermal structure for a prescribed velocity field was determined [e.g. Sleep, 1969, 1975; Kuznir, 1980; Reid and Jackson, 1981]. The models of Sleep [1969, 1975] assume purely horizontal velocities equal to the half spreading rate and include heat resulting from the solidification and cooling of magmatically emplaced crust on the ridge axis. Reid and Jackson [1981] calculated the temperature distribution for mantle flow due to plate spreading on a uniform viscosity half-space as shown in Figure 4a. This model thus includes the effect of vertical mantle flow beneath the ridge axis but ignores the heat resulting from crustal emplacement on the ridge axis. Since both effects are likely to be important, the two models have simply been combined. The velocity field considered is shown by the streamlines in Figure 8a. Crust emplaced on the ridge axis moves horizontally at the half spreading rate, and underlying mantle flows like a uniform viscosity half-space beneath the spreading crust. Heat associated with solidification and cooling of crust on the axis is treated as a concentrated axial heat source distributed over the thickness of the crust, in a manner analogous to that of Sleep [1975]. The crustal thickness (6 km) and deep mantle temperature (1200°C) are prescribed. The temperature of magmatically emplaced material is taken to be greater than the deep mantle temperature by an amount (320°C) representing the heat of fusion of molten basalt (80 cal/g).

The steady state thermal structure was calculated using finite difference approximations with the distribution of grid points shown in Figure 8a. The isotherms of the resulting thermal structure for a half spreading rate of 10 mm/yr are shown in Figure 8b. As inferred from the depth of oceanic intraplate seismicity [Bergman and Solomon, 1984; Weins and Stein, 1984], the bottom of the plate should correspond to a 600°-700°C isotherm. Even at this slow spreading rate, the plate thickness on the ridge axis is significantly less than the crustal thickness. Seismicity at 8-km depths beneath the ridge axis [Toomey et al., 1985] would not be expected on the basis of this model.

Hydrothermal convection of seawater through permeable oceanic crust is widely recognized as an important mechanism of heat transfer, particularly in young oceanic crust. Hydrothermal cooling is one obvious explanation for a narrower magma chamber on fast spreading ridges [Lewis and Garmany, 1982; McClain et al., 1985; Detrick et al., 1986] than would be expected based on thermal models [Sleep, 1975; Kuznir, 1980]. Several studies of hydrothermal convection in a permeable crustal layer have been reported [Ribando et al., 1976; Fehn and Cathles, 1979; Fehn et al. 1983]. However, a recent study by Morton and Sleep [1985] appears to be the only previous study which addresses the effect of hydrothermal cooling on the large-scale thermal structure of a spreading center. Representing hydrothermal cooling as a prescribed distribution of heat sinks within the upper crust, the heat sink distribution was constrained by requiring that the 1185°C isotherm in the models match 2-

to 3-km-deep seismic reflections interpreted to be the top of a magma chamber.

In the following models, to examine the effects of hydrothermal cooling in a simple way, heat transfer due to hydrothermal convection is represented as an increased thermal conductivity. The ordinary thermal conductivity is enhanced by a factor Nu, the Nusselt number for hydrothermal convection in a permeable layer. Rock at a temperature greater than 400°C or at a depth greater than 6 km is assumed to be impermeable because it cannot support open fractures. Since water as hot as 400°C discharges from vents on the seafloor, this a minimum value of the maximum temperature of rock through which water must circulate. Studies of the Samail Ophiolite [Gregory and Taylor, 1981] indicate that subsolidus oxygen isotope exchange with seawater occurred primarily within the upper 5-6 km of the ophiolite, thus giving an estimate of the maximum depth of water penetration.

The thermal models in Figures 8c and 8d were calculated for Nu=3 and 10, respectively, with the same slow spreading rate as in Figure 8b. With Nu=3 the lithosphere, defined by the 600°C isotherm, at the ridge axis remains thinner than the crust. However, with Nu=10, the lithosphere is clearly thicker than the crust and generally consistent with depth of seismicity observed at the Mid-Atlantic Ridge. The plate thickens by about 3 km over a distance of 10 km from the ridge axis. This thickening of the plate with distance from the ridge axis is sufficient for plate extension to contribute significantly to ridge axis topography on slow spreading ridges. For a faster half spreading rate of 50 mm/yr and Nu=10, the lithosphere at the ridge axis remains much thinner than the crust as shown in Figure 8e.

Based on studies of the relationship between Rayleigh number and Nusselt number (cf. Combarnous, 1978, Figure 4), a Nusselt number of 10 for hydrothermal convection in a 6 km thick layer requires a permeability of about 4×10^{-16} m^2, with other values of thermodynamic and transport properties appropriate for water and water-saturated rock in the oceanic crust. Permeability has been inferred or measured in several Deep Sea Drilling Project (DSDP) holes [Anderson and Zoback, 1982; Hickman et al., 1984]. However, the only in situ measurement of permeability at a depth greater than about 600 m in the oceanic crust was obtained at DSDP hole 504B in crust 6.5 m.y. old, several hundred kilometers away from the axis of the Costa Rica Rift on the Galapagos Spreading Center [Anderson and Zoback, 1982]. The measured permeability decreases with depth to a value of 10^{-17} m^2 at depths greater than 500 m. This low value would not account for hydrothermal convective heat transfer with a Nusselt number as large as 10. However, near the ridge axis where active faulting and cracking associated with rapid cooling occur [Lister, 1974], it is not unreasonable to expect larger permeabilities. Further from the axis, cooling cracks and inactive faults are likely to have been filled by hydrothermally deposited minerals.

Thus, if hydrothermal cooling can account for a relatively thick plate near the axis of a slow spreading ridge, the results of the present study suggest that horizontal extensional stresses in a strong plate near the axis of a slow spreading ridge may explain the formation of the axial valley. The transport of magma through the strong mantle layer is a question of obvious importance that is not directly
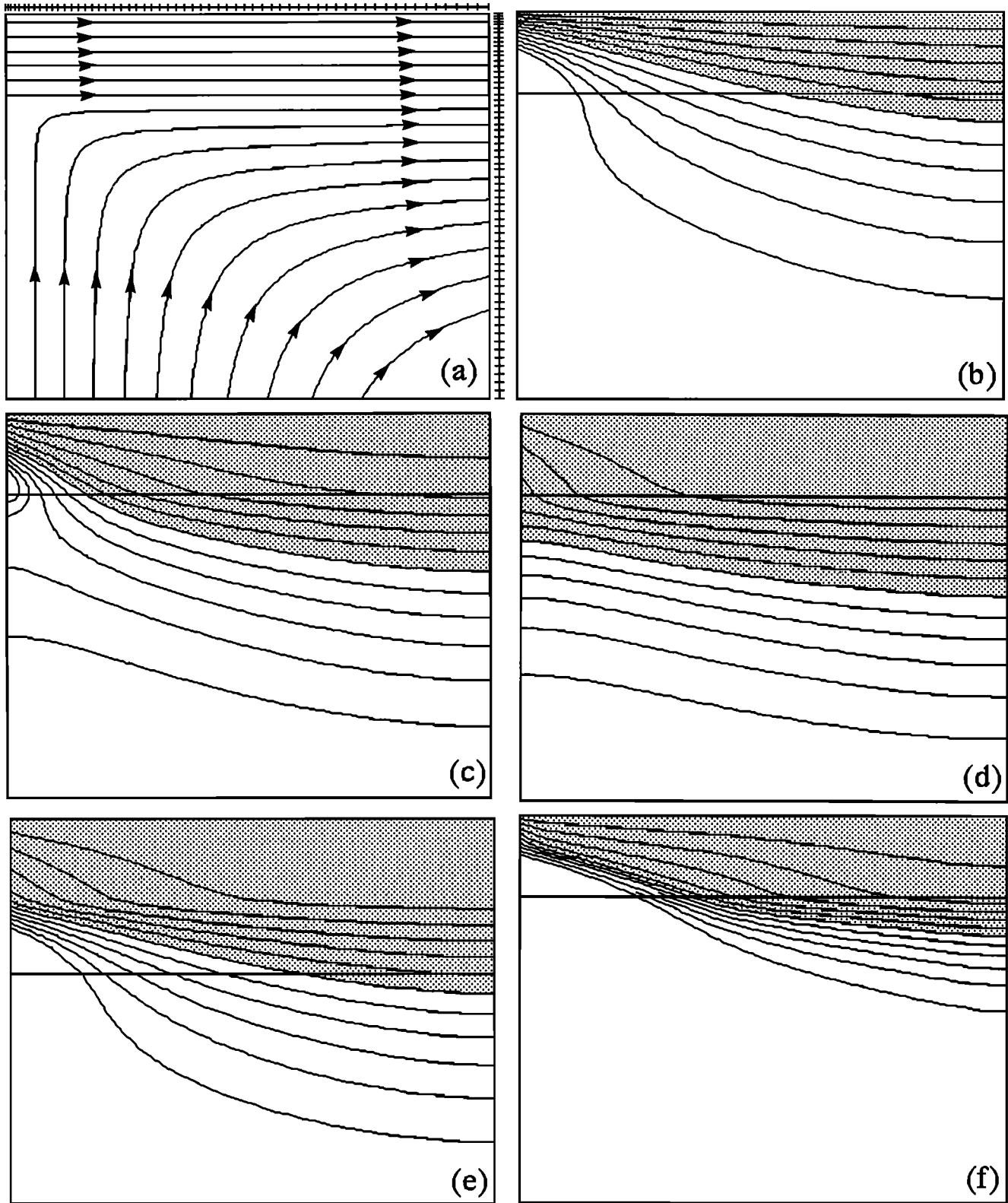
Fig. 8. Mid-ocean ridge thermal structure in a vertical cross section perpendicular to the spreading axis including the effect of hydrothermal cooling. Streamlines of the flow field (Figure 8a) correspond to horizontal motion of crust emplaced on the ridge axis and mantle flow due to plate spreading, like that in Figure 4a, beneath the crust. Grid spacing used in finite difference calculations is shown by tick marks along the sides of the region. Isotherms (Figures 8b-8f) are at temperature intervals of 100°C. Magmatic accretion of the crust on the ridge axis is represented by a heat source that extends to the bottom of the crust. (The base of the crust is shown by the solid horizontal line.) Lithosphere, corresponding to material with a temperature below 600°C, is shaded. Hydrothermal cooling is represented as the ordinary thermal conductivity enhanced by a constant factor Nu representing the Nusselt number for hydrothermal convective cooling. Isotherms are shown for a 10-mm/yr half-spreading rate ridge with $Nu=1$ (Figure 8b), 3 (Figure 8c), and 10 (Figure 8d) and a crustal thickness of 6 km. Isotherms are shown for a 10-mm/yr half-spreading rate ridge with $Nu=10$ (Figure 8e) and a crustal thickness of 12 km; and for a 50-mm/yr half-spreading rate ridge with $Nu=10$ (Figure 8f) and a crustal thickness of 6 km. See text for further discussion.

addressed by the simple models presented above. This may explain episodicity of the spreading process and possibly the large difference in frequency of episodicity inferred for fast and slow spreading ridges [cf. *Macdonald*, 1982]. Magma generated in the upwelling mantle beneath the ridge axis may episodically penetrate the strong plate at the ridge axis in cracklike bodies resulting in periods of reduced extensional stress in the plate near the ridge axis. As shown in Figure 1, volcanism at a ridge axis is restricted to a 1- to 2-km-wide neovolcanic zone that is much narrower than the width of the axial valley and the region of plate extension. If plate extension is to create the stress-supported axial valley, it is sufficient for a continuous strong plate to exist most of the time. During times that magma penetration weakens the plate in a narrow zone at the ridge axis, horizontal extension of the plate outside this region will stop. If the plate behaved as a simple viscous material, the axial valley topography would tend to relax during such times of reduced horizontal extension or stress. However, because the axial valley is produced by faulting, if stresses due to axial valley topography alone are insufficient to cause slip on faults then the axial valley topography will remain frozen-in during these periods of reduced horizontal stress. In our idealized models, stresses due to axial topography are insufficient to cause yielding of the plastic plate. This expected freezing-in of topography is consistent with the observation that extinct slow spreading ridges in the Labrador Sea [*Kristoffersen and Talwani*, 1977], the northeastern Atlantic Ocean [*Talwani and Eldholm*, 1977], and the Coral Sea [*Watts*, 1982] preserve their axial valley morphology and associated gravity anomalies. After extension stopped, the frozen-in topography should be supported by elastic strength of the plate as suggested by *Watts* [1982].

An axial valley that is created by viscous flow in a ridge axis conduit should disappear after spreading stops. The relaxation time required for seafloor elevation at the top of a ridge axis conduit to adjust to changes in pressure within the conduit is $12\mu H/\Delta\rho g d^2$, where H is the conduit height, d is the conduit width, $\Delta\rho$ is seafloor rock-water density difference, and μ is the asthenosphere viscosity [cf. *Phipps Morgan and Parmentier*, 1985]. The depth of the axial valley at a half spreading rate U is $\delta=12\mu UH^2/\Delta\rho g d^3$ [cf. *Parmentier and Forsyth*, 1985] so that the relaxation time becomes simply $\delta d/HU$. For a conduit with $H=30$ km and $d=10$ km (Lachenbruch, 1973), an initially 1-km-deep axial depression at a half spreading rate of 10 mm/yr will relax in approximately 3×10^4 years. The axial valley due to such a ridge axis conduit would be well preserved between spreading episodes occurring each 10^4 years. However, preservation of the axial valley after spreading stops would require cooling and strengthening of mantle material in the ridge axis conduit. The time $H^2/4\kappa$ for conductive cooling to penetrate to a depth H is approximately 8×10^6 years for $H=30$ km and $\kappa=1$ mm^2/s. Even if the upper 5-6 km of the oceanic lithosphere near the ridge axis were rapidly cooled by hydrothermal convection, this cooling time would remain longer than the relaxation time. It therefore appears unlikely that topography produced by a ridge axis conduit would be preserved after spreading stops. If the plate thickness increases more gradually with distance from the ridge axis, as in Figure 3c, the relaxation time for topography supported by mantle flow stresses in a uniform viscos-

ity halfspace is approximately $4\pi\mu/\Delta\rho gL$, where L is the width of the axial valley. With $L=30$ km and $\mu=10^{20}$ Pa s (10^{21} P), as required for mantle flow stresses to produce a 1-km-deep axial valley, the relaxation time is 6×10^4 years.

Clearly, the mechanisms producing the episodic character of spreading require further study. However, axial valley formation by horizontal extensional stresses in a strong plate that deforms by faulting is consistent with episodic spreading and with the preservation of axial topography on extinct ridges.

The axial structure of mid-ocean ridges depends strongly on spreading rate. However, axial structure is also clearly influenced by factors other than the spreading rate. In the vicinity of hot spots where ridge axes are much shallower than normal, an axial valley may not be present even at slow spreading rates. The Reykjanes Ridge is an often cited example. In contrast, at the Australian-Antarctic Discordance, a deeper than normal section of the intermediate spreading rate Australian-Antarctic Ridge, the ridge has a well-defined axial valley that is not present on adjacent sections which are at a more normal depth [*Weissel and Hayes*, 1974; *Forsyth et al.*, 1987]. Ridge axes also deepen systematically approaching a transform fault, and the axial valley becomes correspondingly more pronounced. This correlation of ridge axis structure with seafloor depth may be explained by the relative rates of magmatic heat input associated with crustal formation. In areas where the crustal production rate is low, the seafloor is deep, the magmatic heat input at the ridge axis is low, and the plate is thicker than normal for that spreading rate. The thicker, and therefore stronger, plate will result in a more pronounced axial valley. In contrast, areas of high crustal production will be shallower and will have higher magmatic heat input and therefore thinner ridge axis lithosphere with an axial structure characteristic of a faster spreading rate. This is shown by the example in Figure 8f, where the crustal thickness is double that in Figure 8d while all other parameters of the thermal model remain the same. The lithosphere thickness at the ridge axis was approximately halved by doubling the crustal thickness. For a lithosphere at brittle failure with a frictional strength proportional to depth, halving the lithosphere thickness would decrease the horizontal force and moment by a factor of 4. For a normal crustal thickness at slow spreading rates, as shown in the example of Figure 8d, a significant part of the ridge axis lithosphere will consist of mantle peridotite rather than crustal gabbro. The lower ductile flow strength of gabbro relative to peridotite [*Chen and Morgan*, 1987] would increase the ridge axis weakening effect caused by thickening the crust.

SUMMARY

Axial topography and associated gravity anomalies provide an important constraint on the thermal and mechanical structure of spreading centers. Observed gravity anomalies indicate that the axial topography at slow spreading ridges cannot be isostatically compensated at depths as shallow as 6 km and therefore cannot be simply explained by crustal thickness variations. In this study, several mechanisms for the creation of axial topography at mid-ocean ridges that is supported by stresses within a strong plate near the ridge axis or the flowing mantle beneath it have been examined.

The relative importance of mantle and lithosphere deformation on axial topography has been explored using elementary solutions for viscous flow problems and simple thermal models. The relatively low relief of fast spreading ridges and the pronounced axial valley on slow spreading ridges are the principal features that need to be explained by such first-order models.

A narrow, vertical steady-state conduit through which viscous asthenosphere rises on the ridge axis is an appealingly simple and frequently cited explanation for the presence of an axial valley on slow spreading ridges. However, the temperature field associated with flow in a narrow conduit does not correspond to an assumed steep-walled conduit, but instead has the form of a thermal boundary layer, with nearly horizontal isotherms, that thickens gradually with distance from the ridge axis. Thus if a steady-state ridge axis conduit does exist, the strength difference between asthenosphere and conduit walls must be attributed to a significant strength reduction due to the presence of partial melt in the rising asthenosphere, by an increased strength of depleted residual mantle forming the conduit walls, or by some other, nonthermally controlled mechanism.

Mantle flow due to plate accretion and melt segregation can produce axial-valley-like topography. However, a mantle viscosity beneath the spreading center on the order of 10^{20} Pa s (10^{21} P) is required for these mechanisms to contribute significantly to the kilometer-scale relief present on slow spreading ridges. In the absence of plate accretion and extension near the ridge axis, mantle flow due to plate spreading alone makes no contribution to the topography. This suggests that several previously considered kinematic models based on this mechanism do not adequately explain the axial valley.

Horizontal extensional stresses in a strong, brittle lithosphere that thickens with distance from the ridge axis can produce an axial-valley-like topography with relief comparable to that observed. Using a continuum idealization of deformation due to faulting, the axial valley width is controlled by the plate thickness. A 10-km-thick brittle plate near the ridge axis would produce a 40-km-wide axial valley as observed on slow spreading ridges. Microseismicity, implying brittle plate deformation, has been observed to depths of 8 km at a slow spreading ridge. Based on accepted values for sliding friction on faults, a plate that thickens by as little as several kilometers within the width of the axial valley can produce kilometer-scale relief.

For a transition from strong brittle to weaker ductile deformation that occurs at a relatively constant temperature, the thickness of the plate near a ridge axis is thermally controlled. Thermal models which consider horizontal spreading of magmatically accreted crust on the ridge axis and upwelling mantle flow beneath the axis due to plate spreading predict a plate thickness near the ridge axis that is thinner than the crust even at slow spreading rates. However, including the effect of hydrothermal cooling, represented simply as an enhanced thermal conductivity, a plate thickness of 8 km can be reasonably predicted. These models show that it is reasonable to expect the plate to thicken by at least several kilometers over a horizontal distance of 10 km from the ridge axis. If so, horizontal extensional stresses in lithosphere near the ridge axis can explain both the form and the amplitude of axial valley topography at slow spreading ridges. The same mechanism will operate at fast spreading ridges, but the plate thickness at the ridge axis, as predicted by our models, should be small enough that the horizontal force in the plate is too small to produce appreciable ridge axis relief.

REFERENCES

Anderson, R. N., and M. D. Zoback, Permeability under pressures and convection in the oceanic crust near the Costa Rica Rift, eastern equatorial Pacific, *J. Geophys. Res., 87,* 2860-2868, 1982.

Batchelor, G.K., *An Introduction to Fluid Dynamics,* 615 pp., Cambridge University Press, New York, 1967.

Bergman, E.A., and S.C. Solomon, Source mechanisms of earthquakes near mid-ocean ridges from body waveform inversion: Implications for the early evolution of oceanic lithosphere, *J. Geophys. Res., 89,* 11,415-11,441, 1984.

Brace, W.F., and D.L. Kohlstedt, Limits on lithosphere stress imposed by laboratory experiments, *J. Geophys. Res., 85,* 6248-6252, 1980.

Byerlee, J. D., Friction of rocks, *Pure Appl. Geophys., 116,* 615-626, 1978.

Chen, Y., and W.J. Morgan, A mechanic model for the contrast between the broad rift valleys on slow spreading centers and no valleys on fast spreading ones (abstract), *Eos Trans. AGU, 68,* 407, 1987.

Collette, B. J., J. Verhoet, and A. F. J. de Mulder, Gravity and a model of the median valley, *J. Geophys., 47,* 91-98, 1980.

Combarnous, M., Natural convection in porous media and geothermal systems, *Int. Heat Transfer Conf., 6th,* 45-59, 1978.

Cooper, R. F., and D.L. Kohlstedt, Rheology and structure of olivine-basalt partial melts, *J. Geophys. Res., 91,* 9315-9323, 1986.

Crouch, S. L., and A. M. Starfield, *Boundary Element Methods in Solid Mechanics,* 322 pp., Allen and Unwin, Boston, Mass., 1983.

Detrick, R.S., P. Buhl, J. Mutter, J. Orcutt, T. Brocker, and J. Madsen, Multichannel seismic imaging of the axial magma chamber along the East Pacific Rise between 9 and 13 N (abstract), *Eos Trans. AGU, 67,* 360, 1986.

Fehn, U., and L. M. Cathles, Hydrothermal convection at slow-spreading mid-ocean ridges, *Tectonophysics, 55,* 239-260, 1979.

Fehn, U., K. C. Green, R. P. Von Herzen, and L. M. Cathles, Numerical models for the hydrothermal field at the Galapagos Spreading Center, *J. Geophys. Res., 88,* 1033-1048, 1983.

Forsyth, D.W., R.L. Ehrenbard, and S. Chapin, Anomalous upper mantle beneath the Australian-Antarctic Discordance, *Earth Planet. Sci. Lett.,* in press, 1987.

Gregory, R., and H. P. Taylor, An oxygen isotope profile in a section of Cretaceous oceanic crust, Samail Ophiolite, Oman: Evidence for $\delta^{18}O$ buffering of the oceans by deep (>5 km) seawater-hydrothermal circulation at mid-ocean ridges, *J. Geophys. Res., 86,* 2737-2755, 1981.

Hickman, S. H., M. G. Langseth, J. F. Svitek, In situ permeability and pore pressure measurements near the Mid-Atlantic Ridge, DSDP Site 395, *Initial Rep. Deep Sea Drill. Proj., 78B,* 699-708, 1984.

Karato, S., Does partial melting reduce the creep strength of the upper mantle?, *Nature, 319,* 309-310, 1986.

Kristoffersen, Y., and M. Talwani, Extinct triple junction south of

Greenland and the Tertiary motion of Greenland relative to the North America, Geol. Soc. Am. Bull., 88, 1037-1049, 1977.

Kuznir, N.J., Thermal evolution of the oceanic crust; its dependence on spreading rate and effect on crustal structure, Geophys. J. R. Astron. Soc., 61, 167-181, 1980.

Lachenbruch, A. H., A simple mechanical model for oceanic spreading centers, J. Geophys. Res., 78, 3395-3417, 1973.

Lachenbruch, A. H., Dynamics of a passive spreading center, J. Geophys. Res., 81, 1883-1902, 1976.

Laughton, A.S., and R.C. Searle, Tectonic processes on slow spreading ridges, in Deep Drilling Results in the Atlantic Ocean: Ocean Crust, Maurice Ewing Ser., vol. 2, edited by M. Talwani, C.G. Harrison, and D.E. Hays, pp. 15-32, AGU, Washington, D.C., 1979.

Lewis, B.T.R., and J.D. Garmany, Constraints on the structure of the East Pacific Rise from seismic refraction data, J. Geophys. Res., 87, 8417-8425, 1982.

Lin, J., and E. M. Parmentier, Implications of gravity and topography for the transient thermal and mechanical structure of mid-ocean ridges (abstract), Eos Trans. AGU, 67, 362, 1986.

Lister, C. R. B., On the penetration of water into hot rocks, Geophys. J. R. Astron. Soc., 39, 465-509, 1974.

Louden, K. E., R. S. White, C. G. Potts, and D. W. Forsyth, Structure and seismotectonics of the Vema Fracture Zone, in The Tectonics of Fracture Zones, edited by P.J. Fox, in press, 1987.

Macdonald, K. C., Mid-ocean ridges: Fine scale tectonic, volcanic, and hydrothermal processes within the plate boundary zone, Annu. Rev. Earth Planet. Sci., 10, 155-190, 1982.

Macdonald, K. C., and T. M. Atwater, Evolution of rifted ocean ridges, Earth Planet. Sci. Lett., 39, 319-327, 1978.

Macdonald, K.C., and B. Luyendyk, Deep-Tow studies of the structure of the Mid-Atlantic Ridge crest near 37N (FAMOUS), Geol. Soc. Am. Bull., 88, 621-636, 1977.

McClain, J.S., J.A. Orcutt, and M. Burnett, The East Pacific Rise in cross section: A seismic model, J. Geophys. Res., 90, 8627-8639, 1985.

Morton, J.L., and N.H. Sleep, A mid-ocean ridge thermal model: Constraints on the volume of axial hydrothermal flux, J. Geophys. Res., 90, 11,345-11,353, 1985.

Muskhelishvili, N.I., Some Basic Problems of the Mathematical Theory of Elasticity, 704 pp., Nordhoff, Leyden, Netherlands, 1953.

Nelson, K. D., A simple thermal-mechanical model for mid-ocean ridge topographic variation, Geophys. J. R. Astron. Soc., 65, 19-30, 1981.

Parmentier, E. M., Dynamic topography in rift zones: Implications for lithospheric heating, Philos. Trans. R. Soc. London, Ser. A, 321, 23-25, 1987.

Parmentier, E.M., and D.W. Forsyth, Three-dimensional flow beneath a slow-spreading ridge axis: A dynamic contribution to the deepening of the median valley towards fracture zones, J. Geophys. Res, 90, 678-684, 1985.

Parmentier, E. M., J. Phipps Morgan, and J. Lin, Axial morphology of slow spreading mid-ocean ridges: steady state necking of a ductile lithosphere (abstract), Eos Trans. AGU, 66, 1091, 1985.

Phipps Morgan, J., and E. M. Parmentier, Ridge axis morphology:

Due to mantle deformation? (abstract), Eos Trans. AGU, 65, 1088, 1984.

Phipps Morgan, J., and E. M. Parmentier, Causes and rate-limiting mechanisms of ridge propagation: A fracture mechanics model, J. Geophys. Res., 90, 8603-8612, 1985.

Purdy, G.M., and R.S. Detrick, The crustal structure of the Mid-Atlantic Ridge at 23N from seismic refraction studies, J. Geophys. Res., 91, 3739-3762, 1986.

Reid, I., and H. R. Jackson, Oceanic spreading rate and crustal thickness, Mar. Geophys. Res., 5, 165-172, 1981.

Ribando, R.J., K.E. Torrance, and D.L. Turcotte, Numerical models for hydrothermal circulation in the oceanic crust, J. Geophys. Res., 81, 3007-3012, 1976.

Sleep, N. H., Sensitivity of heat flow and gravity to the mechanism of sea-floor spreading, J. Geophys. Res., 74, 542-549, 1969.

Sleep, N. H., Formation of the oceanic crust: Some thermal constraints, J. Geophys. Res., 80, 4037-4042, 1975.

Sleep, N. H., and B. R. Rosendahl, Topography and tectonics of mid-oceanic ridge axes, J. Geophys. Res., 84, 6831-6839, 1979.

Solomon, S.C., P.Y. Huang, and L. Meinke, The seismic moment budget of slow spreading ridges (abstract), Eos Trans. AGU, 67, 1231, 1986.

Talwani, M., and O. Eldholm, Evolution of the Norwegian-Greenland Sea, Geol. Soc. Am. Bull., 88, 969-999, 1977.

Tapponier, P., and J. Francheteau, Necking of the lithosphere and the mechanics of slowly accreting plate boundaries, J. Geophys. Res., 83, 3955-3970, 1978.

Toomey, D. R., S. C. Solomon, G. M. Purdy, and M. H. Murray, Microearthquakes beneath the median valley of the Mid-Atlantic Ridge near 23N: Hypocenters and focal mechanisms, J. Geophys. Res., 90, 5443-5458, 1985.

Vening Meinesz, F. A., Les graben africains resultat de compression ou de tension dans la croute terrestre, Inst. R. Colon. Belg. Bull. Seances, 21, 539-552, 1950.

Watts, A.B., Gravity anomalies over oceanic rifts, in Oceanic and Continental Rifts, Geodyn. Ser., vol. 8, edited by G. Palmason, pp. 99-106, AGU, Washington, D.C., 1982.

Weissel, J.K., and D.E. Hayes, The Australian-Antarctic Discordance: New results and implications, J. Geophys. Res., 79, 2579-2587, 1974.

Wiens, D.A., and S. Stein, Intraplate seismicity and stresses in young oceanic lithosphere, J. Geophys. Res., 89, 11,442-11,464, 1984.

Zuber, M. T., and E. M. Parmentier, Lithospheric necking: A dynamic model for rift morphology, Earth Planet. Sci. Lett., 77, 373-383, 1986.

J. Phipps Morgan, Department of Earth, Atmospheric and Planetary Sciences, Rm. 54-824, Massachusetts Institute of Technology, Cambridge, MA, 02139

E.M. Parmentier and J. Lin, Department of Geological Sciences, Box 1847, Brown University, Providence, RI, 02912